ISSN 1590-8844
International Journal of Mechanics and Control, Vol. 17, No. 01, 2016

BIOLOGICALLY INSPIRED DESIGN AND HYDRODYNAMIC ANALYSIS OF A REMOTELY OPERATED VEHICLE FOR RIVER UNDERWATER TASKS

Ilija Stevanović* Aleksandar Ćosić* Aleksandar Rodić* Boško Rašuo**

* University of Belgrade, Mihailo Pupin Institute
** University of Belgrade, Faculty of Mechanical Engineering

ABSTRACT

In this paper is presented comparison of two designs of the mechanical structure of river submarine robot dedicated to delicate and risky underwater tasks. The main factors that determine mechanical design of robots are hydrodynamic drags and good mobility in river flow. Robot body design of new robot is inspired by morphological characteristics fast-swimming animals by streamlining the shape of the body by optimising the fineness ratio as the natural geometry proportion that commonly appears with biological systems. Designed mechanical structure is evaluated by corresponding fluid dynamics simulation tests. In the paper is presented the simulation of underwater robots based on mathematical model of real submarine and simple PID controller. Trajectory tracking performance is presented under assumption that the disturbance occurs due to river flow.

Keywords: ROV, UUV, streamlining, PID controller, bionics

1 INTRODUCTION

The subject of research and development presented in this paper regards to prototype development of a remotely operated vehicle (ROV), i.e. unmanned underwater vehicle (UUV) for underwater river tasks. That regards to development of a river underwater robot-grebe intended for remotely operated underwater search, underwater camera shooting, monitoring and inspection of objects and infrastructure installation in the water, rescue missions, ecologic tasks of cleaning and waste disposal removing and sampling of river bottom material as well as assistance in extraction submerged objects from river. The prototype of the underwater robot-explorer is intended for use on big and smooth rivers (not trouble highland waters). That are mainly lowland rivers with large water potential (water flow), whose streaming speed neither overcomes 8 km/h nor depth 20 m. The ROV must be energy efficient and easy to control.

Contact author: Ilija Stevanović[1], Boško Rašuo[2]

[1]Volgina 15, 11060 Belgrade, Serbia.
[2]Kraljice Marije 16, 11060 Belgrade, Serbia.

Energy efficiency is achieved with design of body inspired by nature. Simplified control is achieved with proper position of thrusters for decoupled motion.
The current version of designed ROV is designed based on first version with some improvements.

2 ANALYSIS OF BODY MORPHOLOGY OF FAST-SWIMMING ANIMALS

Fast-swimming animals display morphological characteristics associated with enhanced thrust production, high propulsive efficiency, and reduced drag.
For cetaceans, these morphological characteristics include a streamlined body, tight skin, a strongly compressed caudal peduncle, and high aspect ratio flukes and flippers with sweepback. Drag is minimized primarily by streamlining the shape of the body and appendages (i.e., flukes, flippers, dorsal fin). Streamlining minimizes drag by reducing the magnitude of the pressure gradient over the body and allowing water to flow over the surface without separation.
The streamlined profile is characterized by a fusiform shape emulating an elongate teardrop with a rounded leading edge extending to a maximum thickness and a slowly tapering tail. This fusiform shape is displayed by all cetaceans (Figure 1) [1].

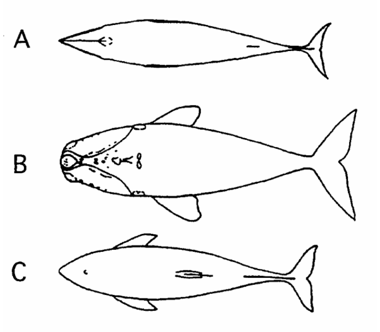

Figure 1 Body shape variation for:
a balaenopterid mysticete (A: *Balaenoptera acutorostrata),*
a balaenid mysticete (B: *Eubalaena glacialis),*
an odontocete (C: *Phocoena phocoena).*

2.1 STREAMLINING – REDUCING DRAG

Drag is minimized primarily by streamlining the shape of the body and appendages (i.e., flukes, flippers, dorsal fin). Streamlining minimizes drag by reducing the magnitude of the pressure gradient over the body and allowing water to flow over the surface without separation. The streamlined profile is characterized by a fusiform shape emulating an elongate teardrop with a rounded leading edge extending to a maximum thickness and a slowly tapering tail. This fusiform shape is displayed by all cetaceans (Figure 1), but is not axisymmetrical, as the caudal peduncle exhibits extreme narrow-necking in the plane of oscillation. Necking in the caudal region reduces virtual mass effects and unstable movements.

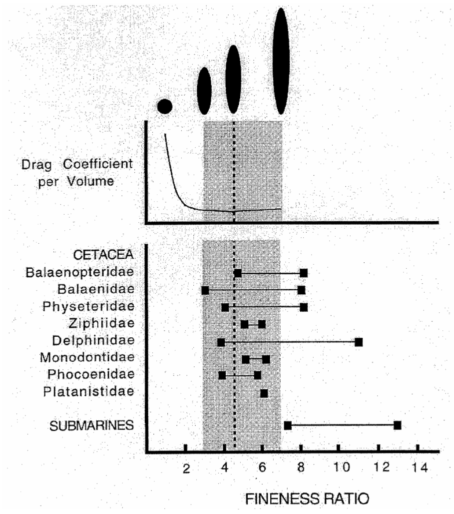

Figure 2. Fineness ratio (FR) in relation to drag per volume (adapted from von Mises, 1945) and FR for cetacean families (adapted from Fish, 1993a). Comparisons are made with modern submarine hulls. Silhouettes show the difference in shape in reference to FR from a circular shape (FR= 1) to an elongate form (FR = 7). The dashed line indicates the optimal FR of 4.5 whereby a body has the lowest drag for the maximum volume. The shaded area represents the FR range (3 through 7) in which drag increases by 10% above the minimum value. [1]

An indicator of the degree of streamlining is the fineness ratio *(FR* = body length/maximum diameter). The *FR* value of 4.5 gives the least drag and surface area for the maximum volume (Figure 2) although only a 10% increase in drag is realized in the *FR* range of 3 through 7. Since Gray (1936), there has been an active search for special mechanisms to reduce drag in dolphins. Despite the various mechanisms hypothesized, the body shape is the major determinant of drag (Figure 2). A stream- lined body with *FR* = 4.5 will have a 75% reduction in pressure drag coefficient from that for a sphere of equal volume.

The *FR* range for the various cetacean families spans a significant portion of optimal range for reduced drag (Figure 2). The greatest range of *FR* (4 through 11) is found in the cetacean family Delphinidae from Dall's porpoise *(Phocoenoides dalli)* to the northern right whale dolphin *(Lissodelphis borealis)*. The exaggerated length of the latter species has given it the name "snake porpoise".

Despite the difference in body design as expressed by *FR,* these two species are considered among the fastest dolphins, with maximum speeds exceeding 8 m/s [1].

3 DESIGN OF ROV's

Two ROV's are designed and analysed in terms of hydrodynamics and control. The ROV's has a task to carry multi-segment, hyper-redundant flexible robot-arm with robot-gripper (Figure 3), different types of sensors (sonars, GPS, etc.), cameras and lights (Figure 5 b). Robot is requested to have fine mobility and manoeuvrability in the water to represents a dexterous underwater device capable to accomplish different underwater tasks. That assumes the robot can move in all directions: up and down, forward and backward, right and left, and twisting about the vertical axis of symmetry.

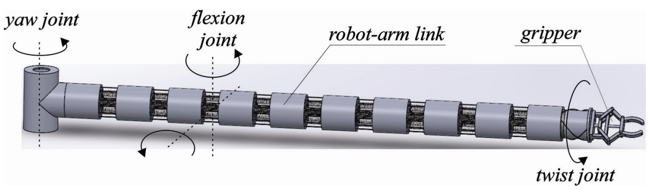

Figure 3 Multi-segment, hyper-redundant flexible robot-arm and robot-gripper

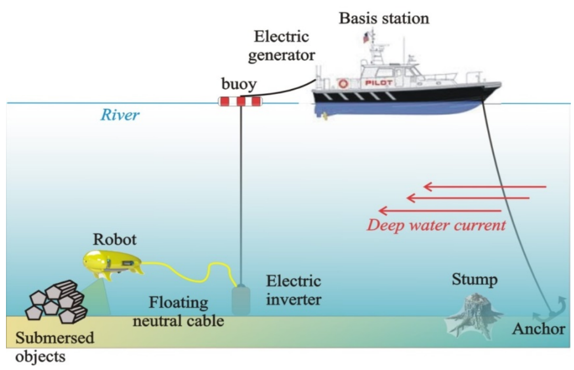

Figure 4 Principle of operation of the ROV – underwater robot.

Principe of operation of ROV – underwater robots are shown on (Figure 4). Robot is permanently in physical contact (connected) with basis station (Figure 4) due to the safety reasons (to prevent loosing), power supply and permanent communication keeping.

3.1 THE ROV 1

For the first ROV design are used streamline fusiform shape with fineness ratio equal to golden ratio (1.61803399) (745x1870x1200mm) and six thrusters.
Thrusters T1-T3 for forward motion and T4 - T6 for up and down motion. No thrusters for lateral motion in direction of X axe (Figure 4), in detail described in [3].

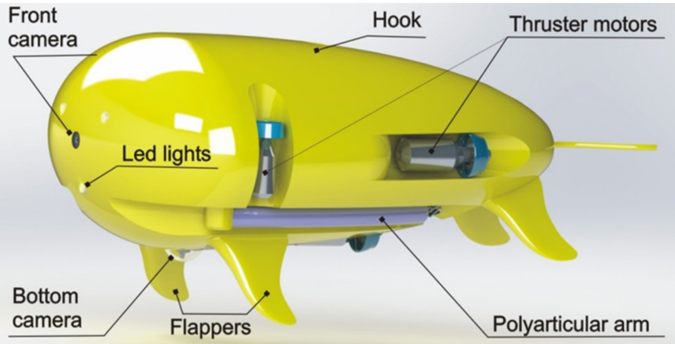

a)

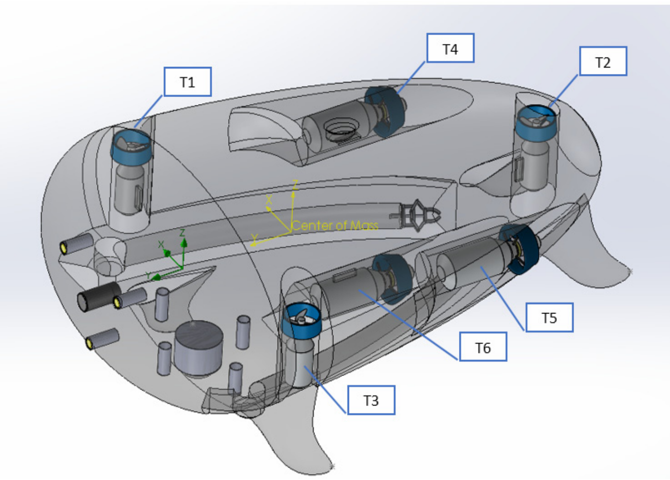

b)

Figure 5 Underwater robot with its components: a) side view; b) x-ray view.

3.2 THE ROV 2

The ROV 2 is designed after analysis of ROV 1. It has all the same requests as the ROV 1. ROV 1 had to be improved in terms of hydrodynamics, better mobility, and manoeuvrability in the water stream.

3.2.1 Streamlining ROV 2

For design of the body of the ROV 2 is used the fineness ratio (FR = body length/maximum diameter) of about 4.5 (240x1400x770 mm).

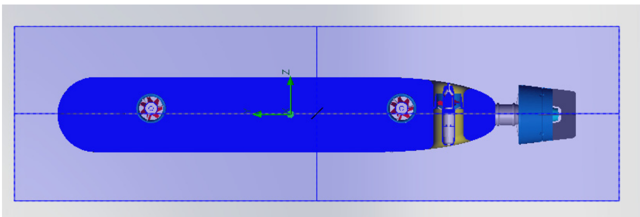

Figure 6 Cross section of ROV 2.

3.2.2 Manoeuvrability ROV 2

In section 6 simulations showed that ROV 1 cannot track spiral trajectory in water stream. Obviously it needs thrusters for lateral motion. However, for stationary water there is no problem for lacking of those thrusters. As a result of all this described ROV 2 is designed. It has 7 thrusters. T1-T3 for up-down motion, T4-T5 for forward-revers and T6-T7 lateral motion (Figure 7).

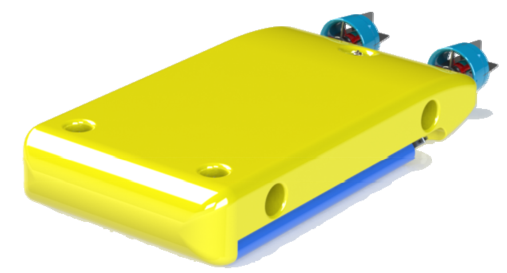

a)

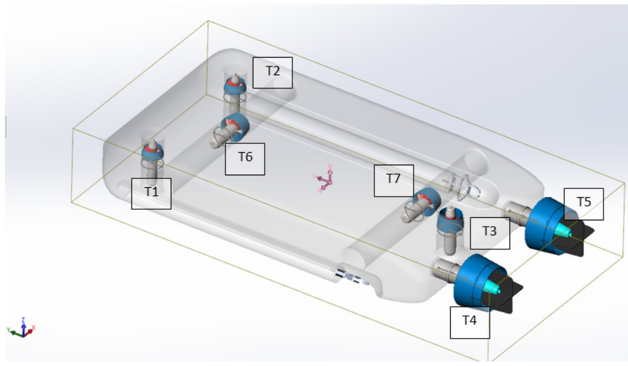

b)

Figure 7 ROV 2: a) side view; b) x-ray view.

The final shape and position of thrusters is logical and very similar as MARUM H-ROV [2]

4 HYDRODYNAMIC ANALYSIS OF ROV's

The hydro dynamically optimized underwater robot (Figure 8 a) and b) is tested up-on the drag forces by modelling in Solidworks. Solidworks Flow Simulation uses Computational Fluid Dynamics (CFD) analysis to enable simulation of fluid flow and to calculate fluid forces and understand the impact of a river stream on ROV performance.

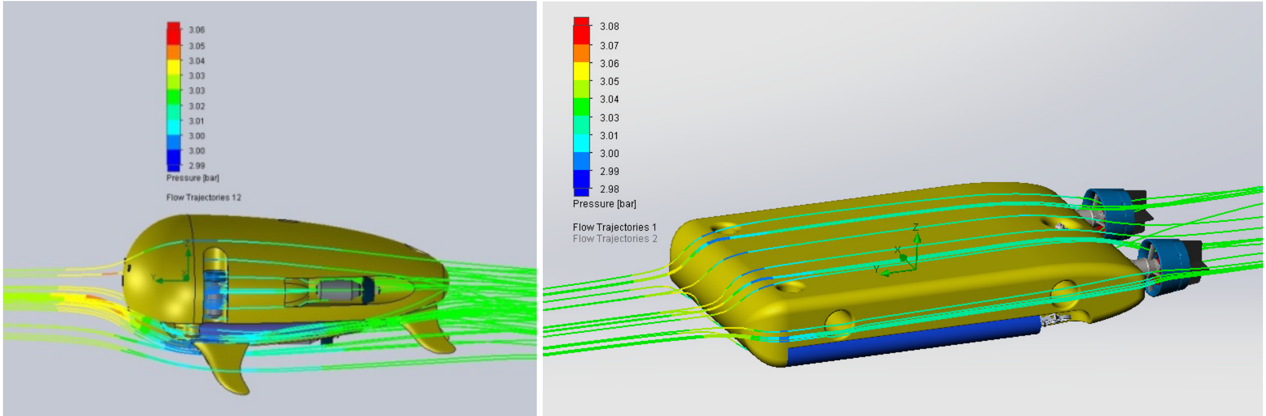

a) b)

Figure 8 Hydrodynamic analysis of the submarine body: a) ROV 1; b) ROV 2.

Tightly integrated with Solidworks CAD, CFD analysis uses Solidworks Simulation flow analysis and reduces the need for costly prototypes, eliminating rework and delays, and saves time and development costs. CFD is a branch of fluid mechanics that uses numerical analysis and algorithms to solve and analyse problems that involve fluid flows. Computers are used to perform the calculations required to simulate the interaction of liquids and gases with surfaces defined by boundary conditions.
The results of this simulation experiment and corresponding streamlines for ROV 1 and ROV 2 are presented in Figure 8 (case when the streaming speed is 10 km/h and the robot keeps position). The so obtained simulation results are systematized (as reported in table I and table II) and based on them thrusters are selected. Than it is analysed again and those results are transferred to Matlab simulation.

5 MODELLING AND CONTROL OF ROV

5.1 DYNAMIC MODEL OF ROV

Mathematical model of the designed underwater vehicle is based on the rigid body kinematics and dynamics. Derivation of the ROV's dynamic model is based on methodology taken from the modelling of serial robotic manipulators, what is comprehensively treated in the [4-6].
In this particular case, ROV can be considered as robot with 6 degrees of freedom (DOFs), i.e. 3 DOFs are prismatic (translation in z, x, and y direction, respectively), while the other 3 DOFs are rotational (yaw, roll and pitch rotations, respectively). Therefore, the robot can be represented by the kinematic chain, depicted in Fig. 9, where the prismatic DOFs are represented by cuboidal elements, whereas rotational DOFs are represented by cylindrical elements.

Table I - ROV 1 hydrodynamic drags obtained by simulation in Solid Works

		Resistance force during the robot movement [N]					
Speed of streaming [km/h]		1	2	3	5	7,5	10
Robot movement direction	Forward	8,355808128	-	75,90494183	210,4932276	461,4344195	804,9717383
	Backward	9,297515187	-	87,22105725	241,1581502	544,6749591	970,8956312
	Laterally	23,5458368	-	213,0559673	-	-	-
	Up	49,29869231	197,0768946	-	-	-	-
	Down	39,22048346	212,0448867	-	-	-	-

Table II - ROV 2 hydrodynamic drags obtained by simulation in Solid Works

		Resistance force during robot movement [N]					
Speed of streaming [km/h]		1	2	3	5	7,5	10
Robot movement direction	Forward	1,9	-	17,4	48,8	111,2	197,4
	Backward	2,6	-	23,9	66,4	150,8	268,0
	Laterally	8,8	-	79,3	-	-	-
	Up	31,1	124,4	-	-	-	-
	Down	39,9	159,7	-	-	-	-

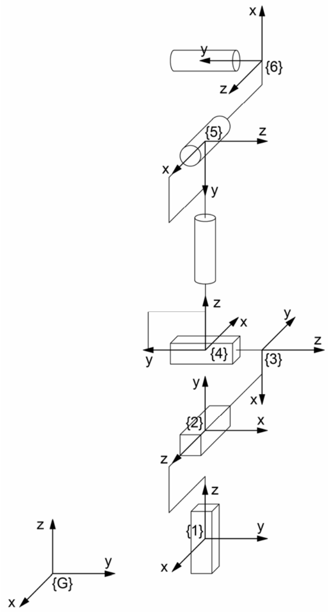

Figure 9 ROV DOFs represented by kinematic chain.

Homogeneous transformations between link frames can be further represented by Denavit-Hartenberg (DH) notation, given in Table III. The global reference frame is static (denoted by {G}), and one frame is assigned to every link according to DH notation. In total, there are 6 frames attached to the links, since there are 6 DOFs, and they are shown in Fig. 9. The pose of the robot corresponds to the pose of the last link frame. It can be noticed from the Table III that the kinematic chain is represented by zero length links, meaning that all the joints lies at a single point, which is the ROV's centre of mass (COM).

Table III – DH parameters

Link no.	DH parameters			
	a	α	d	θ
1	0	$+\pi/2$	q_1	$+\pi/2$
2	0	$-\pi/2$	q_2	$-\pi/2$
3	0	$-\pi/2$	q_3	$+\pi/2$
4	0	$+\pi/2$	0	$q_4-\pi/2$
5	0	$+\pi/2$	0	$q_5+\pi/2$
6	0	$+\pi/2$	0	$q_6+\pi/2$

The whole robot dynamics will be assigned to the last link. Moreover, if the joint coordinates are known, pose of the ROV can be easily determined by forward kinematics [4-6]. Also, if the joint velocities are known, velocity of the ROV can be determined using Jacobian matrix, given by Eq. (1).

$$v = J(q)\dot{q} \tag{1}$$

wherein q denotes vector of generalized coordinates, $\dot{q}$ denotes vector of generalized velocities, v denotes ROV's spatial velocity vector, while *J(q)* stands for Jacobian matrix.

Derivation of the dynamic model follows Lagrangian formulation yielding to a model represented in standard form [7]:

$$M(q)\ddot{q} + C(q,\dot{q})\dot{q} + G(q) - J^T(q)\left[B + W(\dot{q})\right] = \tau \tag{2}$$

wherein the following notation is used: $\ddot{q}$ - vector of generalized accelerations, $M(q)$ - inertial tensor, $C(q,\dot{q})$ - centrifugal and Coriolis matrix, $G(q)$ - gravitational term, $J(q)$ - Jacobian matrix, B - external force due to buoyancy and $W(\dot{q})$ - external force due to the viscous friction during the ROV motion through the fluid.

The Eq. (2) is well known in theory of robotic manipulators and it is comprehensively treated in [4-6]. Comparing the Eq. (2) to the equation of manipulator dynamics, it can be concluded that two external forces are presented, namely, upthrust force (buoyancy) and viscous friction as a result of vehicle motion in the fluid. Buoyancy represents force exerted by fluid and opposing the weight of the ROV submerged in the water. This force always acts in the vertical direction (global frame z direction) and it can be readily calculated using Archimedes' principle.

Unfortunately, it is not the case with the viscous friction, which is not easy to determine. The Eq. (2) denotes so-called inverse dynamics problem. Such a form stands for standardized formulation of robotic manipulators dynamics and it is comprehensively researched and developed.

Once the generalized forces are known, it is necessary to establish relation to the forces of the ROV's thrusters needed to achieve desired generalized forces vector. It can be easily accomplished by employing II Newton's law, therefore, sum of all forces exerted by thrusters must be equal to the force component of the generalized forces vector, and sum of all torques exerted by thrusters with respect to the ROV's COM must be equal to torque component of the generalized forces vector, that is:

$$\sum_i F_i = F_r, \sum_i r_i \times F_i = \tau_r \tag{3}$$

where terms F_i denote forces exerted by thrusters, F_r denotes force component of the generalized forces vector, while terms r_i denote radius vectors of thrusters with respect to ROV's COM and τ_r denotes torque component of the generalized forces vector. At the end, derived relation is linear and can be written in the matrix form:

$$\mathbf{A} \cdot \mathbf{F} = \boldsymbol{\tau}, \mathbf{F} = \begin{bmatrix} F_1 & \cdots & F_n \end{bmatrix}^T, \boldsymbol{\tau} = \begin{bmatrix} F_r \\ \tau_r \end{bmatrix} \tag{4}$$

where n denotes the total number of thrusters used for ROV actuation. Let us take a closer look at matrix **A**. In the first (ROV 1) case, the robot is not actuated along local x axis, and consequently *rank*(**A**)=5, yielding to underactuated system, since the first row of the matrix **A** contains all zeros. Therefore, due to nature of the actuating system, generalized force component along local x axis cannot be controlled and the robot is heavily affected by disturbances acting in that particular direction, which are always present in river flows. On the other hand, in the second design case (ROV 2), *rank*(**A**)=6, yielding to fully actuated system.

However, solving Eq. (4) in both design cases is not straight forward, since in the first design case we have 5 equations with 6 unknowns, while in the second design case we have 6 equations with 7 unknowns. Therefore, in both design cases, we can use the same solving technique. In both design cases, one unknown more provides additional degree of freedom which allows us to optimize control of thrusters with certain aim. The objective is to find the solution which minimizes energy consumption. Thus, the problem can be stated as minimization under linear constraint, that is:

$$\begin{gathered}\mathbf{F}^* = \arg\min_{\mathbf{F}} \|\mathbf{F}\|_W = \arg\min_{\mathbf{F}} \mathbf{F}^T W \mathbf{F}, \\ \text{constraint}: \mathbf{A}\cdot\mathbf{F} = \boldsymbol{\tau}\end{gathered} \tag{5}$$

where W is diagonal weight matrix. Note that the minimization criterion is quadratic form with respect to **F**, and the constraint is linear. Such a problem can be solved by using method of Lagrange multipliers. The first step involves creating Lagrangian L(F,λ) and solving system of generally nonlinear equations:

$$\begin{gathered}\mathrm{L}(\mathbf{F},\lambda) = \mathbf{F}^T W \mathbf{F} - \lambda(\mathbf{A}\cdot\mathbf{F} - \boldsymbol{\tau}) \\ \frac{\partial \mathrm{L}(\mathbf{F},\lambda)}{\partial \mathbf{F}} = 0,\ \mathbf{A}\cdot\mathbf{F} = \boldsymbol{\tau}\end{gathered} \tag{6}$$

The obtained solution minimizes weighted energy criterion, given by Eq. (5).

5.2 TRAJECTORY TRACKING CONTROLLER

In order to tackle trajectory tracking problem, simple decentralized proportional-integral-derivative (PID) controller has been designed. In order to control the pose of the underwater robots, various control laws can be introduced [7-8]. However, PID control is chosen due to its simplicity and wide variety of different applications in industry [9]. Moreover, if the model given by Eq. (2) is chosen, PD control with appropriately adjusted gains guarantee asymptotic stability of the closed loop system in the absence of viscous friction term. The basic block scheme of the closed loop control system is depicted in Fig. 10, where the following notation is adopted: K_p - proportional gain, K_d - differential gain, K_i - integral gain, q^* - desired joint coordinates, $\ddot{q}^*$ - desired joint accelerations, e - error vector and τ_c - control vector which represents generalized forces further transformed to the thruster forces by employing Eq. (6) and applied by the thruster motors.

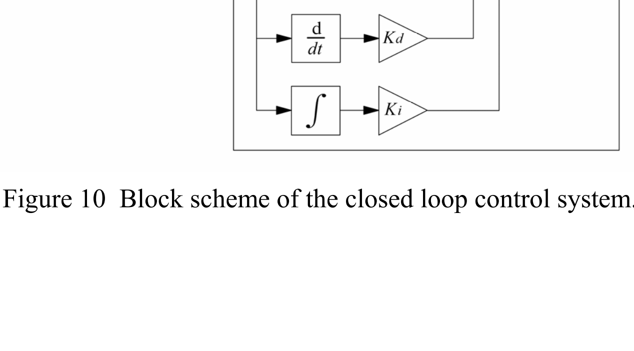

Figure 10 Block scheme of the closed loop control system.

Since the robot has 6 DOFs, PID controller has also 6 DOFs and the corresponding proportional, integral and differential gain matrices are 6x6 diagonal matrices. Therefore, control τ_c corresponds to the generalized forces vector, evaluated by the following expression:

$$\tau_c = \ddot{q}^* + K_p e + K_d \dot{e} + K_i \int e \cdot dt \tag{7}$$

Once the control is determined, the thruster forces can be easily obtained by employing Eq. (6).

As previously mentioned, for the ROV 1, gains corresponding to the generalized force component acting in the local x direction must be set to zero, since the robot is not actuated along that particular direction. This is not the case for the ROV 2, since the robot is fully actuated.

6 SIMULATION RESULTS

In this section, simulation results will be presented and compared for the ROVs 1 and 2. Simulation has been carried out in Mathworks MatLAB environment, using Robotics toolbox [5], [10]. In both cases, it is assumed that the ROV's motion has been carried out in the river, and the river flow course is constant with respect to the global frame of reference. It is further assumed that the speed of river flow is 0.42*m/s* and directed at angle of 45° with respect to the x axis of the global reference frame. Modelling hydrodynamic drag is not trivial and it is conducted by the means of Dassault Systemes SolidWorks. Generally speaking, it is proportional to the squared speed of the vehicle, its cross sectional area and surrounding fluid density. It also depends on shape of the object and roughness of its surface. Trajectory tracking performance is assessed considering spiral desired trajectory, that is, ROV slowly dives following spiral trajectory, described by the following parametric equation:

$$\begin{gathered}x(t) = R_x \cos(\omega t + \phi_0) + x_0 \\ y(t) = R_y \sin(\omega t + \phi_0) + y_0 \\ z(t) = ct + z_0\end{gathered} \tag{8}$$

where $(R_x, R_y) = (5,4)m$ denotes the major and minor axes of the ellipse obtained by projecting spiral onto xy plane, $(x_0, y_0, z_0) = (0,0,0)$ denotes centre of the spiral in 3D space, $\omega = 0.0781 rad/s$ stands for angular velocity, whereas the $c = -0.02 m/s$ is the diving speed. Parameters are chosen such that the ROV's speed is approximately 0.5*m/s*. Eq. (8) defines only desired position of the ROV's COM in the 3D space, while the desired ROV's orientation is yet to be defined. However, careful examination of desired orientation is very important since the hydrodynamic drag is not equal in all directions during motion. Therefore, it is very important to determine desired orientation along trajectory in a way to decrease disturbance due to hydrodynamic drag, but bearing on mind that the ROV is designed in a way that it is the most hydrodynamic when it moves straight forward.

Taking that into account, we adopted that the y axis of the ROV's frame is tangent to the trajectory and that x axis lies in the xy plane of the global reference frame. Moreover, in order to assess tracking performance fairly, both ROVs start at the same initial point $X_0 = [5.5 \quad -0.5 \quad 0.2]^T\ m$ and the same initial orientation $\psi = [0 \quad 0 \quad 0]^T\ rad$ defining initial roll, pitch and yaw angles. Physical dimensions of the designed ROVs are given by Table IV, together with corresponding masses and volumes, and thruster limits. In both cases, PID tracking controllers are tuned manually, trying to make balance between trajectory tracking performance and disturbance rejection. In addition, diagonal weight matrices are chosen to be the same for ROV 1 and ROV 2 and equal to identity matrix, meaning that action of all the thrusters is equally penalized.

Table IV – ROVs physical parameters

parameter	ROV 1	ROV 2
mass	88kg	58.3kg
total volume	0.768m^3	0.0589 m^3
dimensions (length x width x height)	1.87x1.2x0.745m	1.4x0.77x0.24m
number of thrusters	6	7
thruster limits	(25.5, 25.5, 25.5, 12.4, 12.4, 12.4)kg	(2.1, 2.1, 5.4, 25, 25, 10, 10) kg

6.1 TRACKING PERFORMANCE FOR ROV 1

Trajectory tracking performance for ROV 1 is given by Figs. 11-14. Fig. 11 shows tracking performance regarding x, y and z direction and roll (R), pitch (P) and yaw (Y) angles. Desired values are shown by dashed lines, whereas the achieved ones are shown by solid lines. Tracking errors along x, y and z axes and regarding roll (R), pitch (P) and yaw (Y) angles are presented in Fig. 12. Finally, thruster forces are given in Fig. 13, while the achieved trajectory in 3D space is shown in Fig. 14.

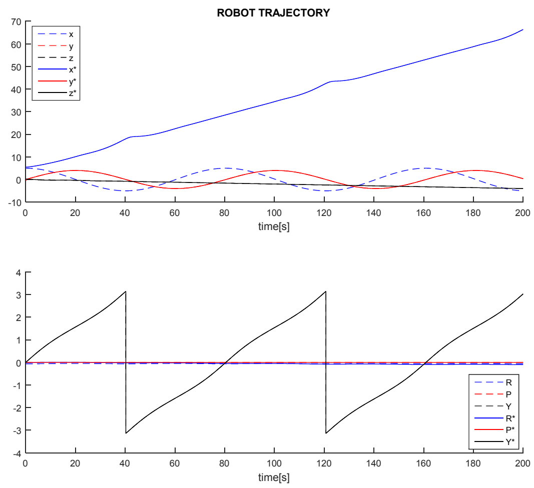

Figure 11 Trajectory tracking performance for ROV 1.

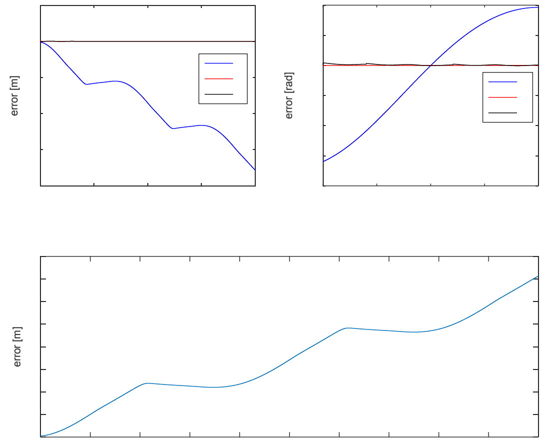

Figure 12 Tracking error for ROV 1.

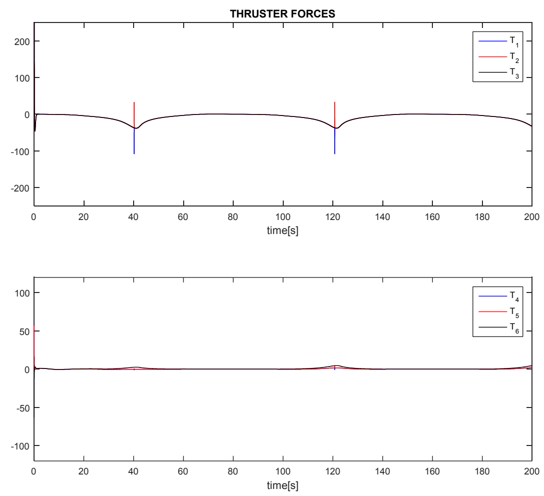

Figure 13 Thruster forces during tracking for ROV 1.

First of all, hydrodynamic drag can be considered as disturbance acting at the input of the system. If the vehicle is fully submerged, buoyancy is constant and known, and therefore, it is easy to compensate for it. Hence, control objective becomes ensuring trajectory tracking, together with disturbance rejection due to hydrodynamic drag.

It is evident that the error along x direction cannot be controlled if the disturbance is presented, since the ROV lacks actuation along that direction. Therefore, motion along y and z direction, and roll, pitch and yaw angles is stabilized, since those errors are kept small. However, error along x axis diverge, meaning that river carries ROV away from the desired position considering x direction. This statement can be clearly seen in Fig. 14. At the end, thruster forces are kept inside their limits, meaning that the motors are chosen appropriately. Peak in the control signal happens whenever ROV's yaw coordinate switches from 2π to 0 rad, and it is additionally increased by derivative action.

6.2 TRACKING PERFORMANCE FOR ROV 2

Trajectory tracking performance for ROV 2 is given by Figs. 15-18, which follow the same order and notation compared to the results for ROV 2. It is immediately noticed from Figs. 12 and 16, that the tracking performance is much better due to side thrusters which provide full actuation of the system. In the case of ROV 1 error diverge, oppositely to ROV 2 case where the error gradually vanishes as the motion evolves. Thruster forces remains inside their limits, therefore, the actuators are appropriately chosen. At the end, we conclude that the ROV 2 is better suited for tracking purposes, providing accurate trajectory tracking and disturbance rejection. However, ROV 1 can be used in calm waters, where the disturbance due to water motion is not considerable.

7 HYDRODYNAMIC ANALYSIS OF ROV's

Designing underwater river ROV by using analysis of bodies of fast-swimming animals and Solidworks CFD in cooperation of Matlab simulation of motion dynamics are resulted with improved performances of ROV 2. Behaviour of both ROVs has been examined in the simulations.

The performance of proposed designs is evaluated in trajectory tracking applications. ROV 2 outperforms ROV 1 in the river environments, where considerable disturbances occur.

Due to full actuation, ROV 2 is able to accurately track assigned trajectory and reject disturbances due to water flow. Oppositely, ROV 1 is underactuated system and tracking error diverges when significant disturbances occur along non-actuated DOF. Still, it is suitable for calm waters where the disturbances are not considerable.

ACKNOWLEDGEMENT

This work is supported by Ministry of Science Ministry of Education, Science and Technology Development of the Republic of Serbia under the grant TR-35003.

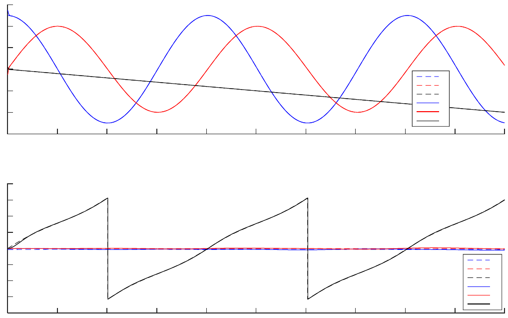

Figure 15 Trajectory tracking performance for ROV 2.

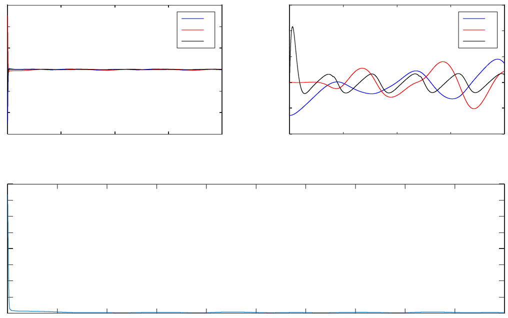

Figure 16 Tracking error for ROV 2.

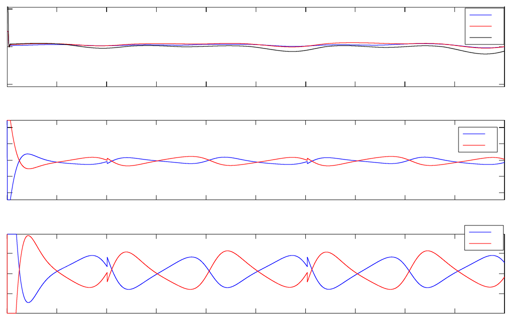

Figure 17 Thruster forces during tracking for ROV 2.

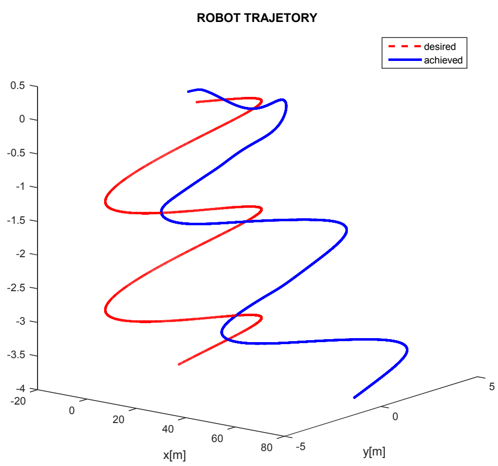

Figure 14 Trajectory achieved by ROV 1.

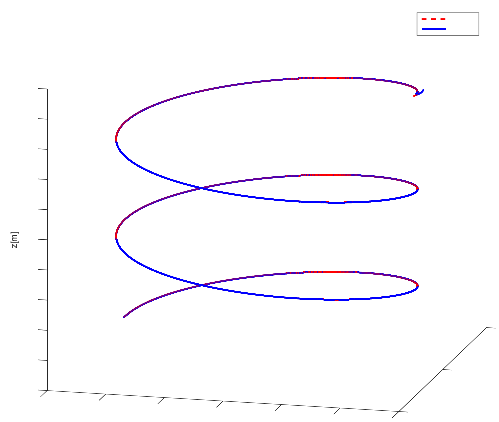

Figure 18 Trajectory achieved by ROV 2.

REFERENCES

[1] Fish F.E., Rohr J., *Review of Dolphin Hydrodynamics and Swimming Performance*. SSC San Diego, 1999.

[2] Meinecke G., Ratmeyer V., Renken J., HYBRID-ROV Development of a new underwater vehicle for high-risk areas. *Oceans'11mts/kona*, Vol. 1, No. 1, pp. 1-6, 2011.

[3] Rodić A., Stevanović I., Jovanović M., Urukalo Đ., On building remotely operated underwater robot-explorer with bi-manual poly-articular system, *Proceedings of Robotics in Alpe-Adria-DAnubae region (RAAD 2015),* Bucharest, pp. 1-8, 27-5, 2015.

[4] Paul R.B., *Robot Manipulators: Mathematics, Programming and Control*, 1st ed., MIT Press, Cambidge, MA, USA, 1982.

[5] Corke P., *Robotics, Vision and Control: Fundamental Algorithms in MATLAB*, Springer-Verlag Berlin Heidelberg, 2011.

[6] Siciliano B., Khatib O., *Springer Handbook of Robotics*, Springer-Verlag Berlin Heidelberg, 2008.

[7] Yuh J., Design and Control of Autonomous Underwater Robots: A Survey, *Autonomous Robots,* Vol. 8, No. 1, pp. 7-24, 2000.

[8] Valavanis K.P., Gracanin D., Matijasevic M., Kolluru R. and Demetriou G. A., Control architectures for autonomous underwater vehicles, *IEEE Control Systems*, Vol. 17, No. 6, pp. 48-64, 1997.

[9] Astrom K.J., Hagglund T., *PID Controllers – Theory, Design and Tuning,* 2nd edition, ISA, New York, USA, 1995.

[10] Corke P.I, MATLAB Toolboxes: Robotics and Vision for Students and Teachers, *IEEE Robotics and Automation Magazine,* Vol. 14, No. 4, pp. 16-17, 2007.